Translational Oncology 14 (2021) 101198

Contents lists available at ScienceDirect

Translational Oncology

journal homepage: www.elsevier.com/locate/tranon

Evolutionary dynamics of cancer multidrug resistance in response to olaparib and photodynamic therapy

Baglo Yan[a], Aaron J. Sorrin[a,1], Pu Xiaocong[a,1], Liu Cindy[a], Jocelyn Reader[b,c], Dana M. Roque[b,c], Huang-Chiao Huang[a,c,*]

[a] Fischell Department of Bioengineering, University of Maryland, College Park 20742 MD, USA
[b] Department of Obstetrics, Gynecology and Reproductive Sciences, University of Maryland School of Medicine, Baltimore 21201 MD, USA
[c] Marlene and Stewart Greenebaum Cancer Center, University of Maryland School of Medicine, Baltimore 21201 MD, USA

ARTICLE INFO

Keywords:
Multidrug resistance
ATP-binding cassette transporters
Photodynamic therapy
Poly (ADP-ribose) polymerase inhibitors
Cancer evolution

ABSTRACT

P-glycoprotein (P-gp) is an adenosine triphosphate (ATP)-dependent drug efflux protein commonly associated with multidrug resistance in cancer chemotherapy. In this report, we used a dual-fluorescent co-culture model to study the population dynamics of the drug sensitive human ovarian cancer cell line (OVCAR-8-DsRed2) and its resistant subline that overexpresses P-gp (NCI/ADR-RES-EGFP) during the course of a photodynamic therapy (PDT)-olaparib combination regimen. Without treatment, OVCAR-8-DsRed2 cells grew more rapidly than the NCI/ADR-RES-EGFP cells. Olaparib treatment reduced the total number of cancer cells by 70±4% but selected for the resistant NCI/ADR-RES-EGFP population since olaparib is an efflux substrate for the P-gp pump. This study used the FDA-approved benzoporphyrin derivative (BPD) photosensitizer or its lipidated formulation ((16:0)LysoPC-BPD) to kill OVCAR-8 cells and reduce the likelihood that olaparib-resistant cells would have selective advantage. Three cycles of PDT effectively reduced the total cell number by 66±3%, while stabilizing the population ratio of sensitive and resistant cells at approximately 1:1. The combination of olaparib treatment and PDT enhanced PARP cleavage and deoxyribonucleic acid (DNA) damage, further decreasing the total cancer cell number down to 10±2%. We also showed that the combination of olaparib and (16:0)LysoPC-BPD-based PDT is up to 18-fold more effective in mitigating the selection of resistant NCI/ADR-RES-EGFP cells, compared to using olaparib and BPD-based PDT. These studies suggest that PDT may improve the effectiveness of olaparib, and the use of a lipidated photosensitizer formulation holds promise in overcoming cancer drug resistance.

Introduction

Ovarian cancer is a dynamic ecosystem where populations of cells with specific genetic and molecular determinants constantly predominate as the disease progresses [1,2]. Although many effective treatments are available for cancer patients, the development of multidrug resistance (MDR) frequently occurs (up to 80–90% for ovarian cancer) and ultimately leads to disease progression and patient death in most cases [3,4]. This is in part because the majority of existing anti-cancer drugs target the larger population of sensitive cells, leaving behind resistant clones to proliferate with less competition for resources [5]. While the development of MDR seems to be nearly inevitable, it need not be insurmountable if the process of selection for resistant cancer populations can be redirected or impeded. It is becoming increasingly clear that combination therapies with non-overlapping mechanisms of action are most likely to delay or even prevent the emergence of resistant

Abbreviations: (16:0)LysoPC, 1-palmitoyl-2-hydroxy-sn-glycero-3-phosphocholine; ATP, Adenosine triphosphate; ABC, ATP-binding cassette; BPD, Benzoporphyrin derivative; DNA, Deoxyribonucleic acid; DMSO, Dimethyl sulfoxide; FACS, Fluorescence-activated cell sorting; OVCAR-8-DsRed2, Human ovarian cancer cell line OVCAR-8 expressing *Discosoma* sp. red fluorescent protein; MDR, Multidrug resistance; NCI/ADR-RES-EGFP, Multidrug resistant OVCAR-8 subline overexpressing P-gp and enhanced green fluorescent protein; ANOVA, One-way analysis of variance; P-gp, P-glycoprotein; PBS, Phosphate-buffered saline; PDT, Photodynamic therapy; PE, Plating efficiency; PARP, Poly(ADP-ribose) polymerase; RIPA buffer, Radioimmunoprecipitation assay buffer; ROS, Reactive oxygen species; SF, Survival fraction; TBST, Tris-buffered saline with 0.1% Tween® 20 Detergent; FDA, U.S. Food and Drug Administration.

* Corresponding author at: 8278 Paint Branch Drive, College Park, MD 20742, USA.
E-mail address: hchuang@umd.edu (H.-C. Huang).

[1] These authors contributed equally to this work.

https://doi.org/10.1016/j.tranon.2021.101198
Received 26 May 2021; Received in revised form 15 July 2021; Accepted 8 August 2021

clones, turning cancer into a manageable chronic disease [6,7]. Ideally, these anti-cancer drugs or regimens should also be delivered with low overlapping-toxicities to improve the patient's quality of life. This study provides new insights into the evolutionary dynamics of MDR in response to olaparib therapy, photodynamic treatment, and their effective combination in ovarian cancer cells.

The expression of adenosine triphosphate (ATP)-binding cassette (ABC) drug transporters in cancer cells has been linked to MDR and poor patient outcomes. These drug transporter proteins utilize energy from ATP binding and hydrolysis to efflux various compounds across cell membranes [8–10]. P-glycoprotein (P-gp, encoded by the *ABCB1* gene) is one of the ABC transporters that has been shown to efflux many drugs (e.g., taxanes, camptothecins, olaparib) out of ovarian cancer cells. Olaparib is a poly(ADP-ribose) polymerase (PARP) inhibitor that was initially developed for the treatment of high-grade ovarian cancers with a germline or somatic *BRCA* mutation, but was updated to include approval for use in all platinum-sensitive relapsed ovarian cancers [11]. The anti-cancer activity of olaparib is mediated through a process called synthetic lethality [12,13]. Olaparib inhibits and traps PARP at the sites of deoxyribonucleic acid (DNA) single-strand breaks during DNA replication, repair, and transcription. This prevents DNA repair and leads to the generation of DNA double-strand breaks. In homologous recombination-proficient cancer patients, DNA double-strand breaks can be repaired efficiently. However, in patients with *BRCA1* or *BRCA2* mutations, DNA double-strand breaks cannot be repaired, leading to genomic instability and eventual cancer cell death. The SOLO-1 trial showed that olaparib maintenance therapy improved the median progression-free survival from 13.8 months to 49.9 months in patients with newly diagnosed advanced ovarian cancer and a *BRCA1/2* mutation [14]. In addition, the Study 19 trial showed that olaparib improved the progression-free survival in the overall patient population with platinum-sensitive relapsed ovarian cancer (hazard ratio 0.35) and had an even greater effect on patients with *BRCA* mutation (hazard ratio 0.18) [11]. While olaparib provided a significant progression-free survival benefit with a relatively low discontinuation rate (12%), the full potential of olaparib could still be hindered by ABC transporter (P-gp)-mediated drug efflux since it is a known substrate for this efflux pump [15,16]. It has also been suggested that multidrug resistant cells may be hypersensitive to metabolic perturbations as they require extra energy to support drug resistance mechanisms [17–20]. This study exploits these weaknesses using clinically relevant photodynamic treatment, aiming to modulate the evolution of cancer cell populations and mitigate MDR.

Photodynamic therapy (PDT) is a photochemistry-based modality that is mechanistically distinct from conventional chemotherapy, radiation, and immunotherapy [21]. PDT involves light activation of photosensitive molecules, also called photosensitizers, to generate reactive oxygen species (ROS) that induce cell death or modulate cell phenotype. The cytotoxicity from PDT is governed by the localization of the photosensitizer, spatial confinement of light, and the short distances over which the ROS remain active. One of the preferential sites of localization of benzoporphyrin derivative (BPD), a U.S. Food and Drug Administration (FDA)-approved photosensitizer used in the present study, is the mitochondrion [22–26]. Light activation of BPD can induce photodynamic disruption of the mitochondrial membrane, which triggers the release of cytochrome c, a potent initiator of apoptotic cell death [22–26]. This direct pathway to cell death suggests that PDT is effective even against chemoresistant cancer cells characterized by defective signaling pathways, as long as there is sufficient light and intracellular photosensitizer. BPD-based PDT has been shown to reverse chemoresistance, synergize with chemotherapy and biological agents, and improve drug transport to tumors [27–32]. It has also been demonstrated that BPD-based PDT can mitigate the surges in pro-tumorigenic CD44 and CXCR4 expression in human pancreatic tumors after multiple cycles of chemotherapy [33]. Recently, we discovered that BPD is a substrate of P-gp, and cancer cells that overexpress P-gp can reduce the intracellular BPD accumulation, mitigating PDT efficacy [34]. To overcome these challenges, a new lipidated formulation of BPD has been developed to reduce BPD efflux by P-gp in cancer cells and improve PDT outcomes [34]. In this study, we compared the ability of BPD and lipidated BPD to photodynamically modulate the population dynamics of sensitive and resistant human ovarian cancer cells.

Here, we investigated the population dynamics of sensitive and resistant ovarian cancer cell lines during the course of olaparib therapy, PDT, and their combination. To capture the growth dynamics of resistant and sensitive ovarian cancer populations, we used a co-culture model of two fluorescent cell lines: (1) the drug sensitive human ovarian cancer cell line OVCAR-8 expressing *Discosoma* sp. red fluorescent protein (OVCAR-8-DsRed), and (2) its multidrug resistant subline expressing P-gp and enhanced green fluorescent protein (NCI/ADR-RES-EGFP). Notably, OVCAR-8 exhibits methylation of *BRCA1* with corresponding reductions in gene expression and heightened sensitivity to PARP inhibition relative to wild-type ovarian cancer cell lines [35].

Materials and methods

Chemicals

The photosensitizer benzoporphyrin derivative (BPD) was purchased from the United States Pharmacopeia (Rockville, MD). The phospholipid, 1-palmitoyl-2-hydroxy-sn-glycero-3-phosphocholine ((16:0) LysoPC), was obtained from Avanti® Polar Lipids (Alabaster, Alabama). The (16:0)LysoPC-BPD conjugates were prepared by crosslinking the carboxylic acid group of the BPD to the hydroxyl function group of (16:0)LysoPC via esterification reaction as described previously [34]. Olaparib (AZD2281) was purchased from Adooq® Bioscience (Irvine, CA) and dissolved with sterile dimethyl sulfoxide (DMSO).

Cell culture

The high-grade serous parental human ovarian cancer cell line OVCAR-8 expressing *Discosoma* sp. red fluorescent protein (OVCAR-8-DsRed2) and the multidrug resistant subline overexpressing P-gp and enhanced green fluorescent protein (NCI/ADR-RES-EGFP) were gifted to the Huang Lab from Dr. Michael M. Gottesman (Laboratory of Cell Biology, Center for Cancer Research, National Cancer Institute, National Institutes of Health, Baltimore, MD). The development and validation of the fluorescent OVCAR-8-DsRed2 and NCI/ADR-RES-EGFP cell lines were described previously. The growth kinetics of OVCAR-8-DsRed2 and NCI/ADR-RES-EGFP were found to be similar to their non-transfected parental cells [36]. The cell lines were cultured in RPMI 1640 medium supplemented with 10% fetal bovine serum and 1% penicillin and streptomycin. The fluorescent cells were initially enhanced once with 500 μg/mL and 200 μg/mL of G418 (Invitrogen) for OVCAR-8-DsRed2 and NCI/ADR-RES-EGFP lines, respectively. All cell lines were confirmed to be mycoplasma-free and maintained at 37°C in a humidified atmosphere containing 5% CO_2.

Cell growth evaluation and flow cytometry analysis

Growth curves were characterized by seeding OVCAR-8-DsRed2, NCI/ADR-RES-EGFP, or their mixtures (1:1 ratio) at different cell numbers (1×10^4 to 2×10^5) in 35-mm Petri dishes for 7 days. For extended cell culture beyond 7 days, cells were reseeded at a density of 5×10^4. The G418-free cell culture media was changed every 2 days followed by fluorescence imaging of OVCAR-8-DsRed2 and NCI/ADR-RES-EGFP cells using a Lionheart™ FX Automated Microscope (Biotek, Winooski, VT) with RFP and GFP filters. Cells were trypsinized and harvested on different days, and total cell counts were assessed by a Cellometer® Automatic Cell Counter (Cellometer Auto T4; Nexcelcom, Lawrence, MA). For flow cytometry analysis of OVCAR-8-DsRed2 and NCI/ADR-RES-EGFP mixed populations, trypsinized cells were washed

and resuspended with 1 mL of cold 0.1% fetal bovine serum in phosphate-buffered saline (PBS), and then analyzed on a fluorescence-activated cell sorting flow cytometer (BD FACScanto™ II; San Jose, CA). The DsRed2 and EGFP fluorescence signals were detected with a 488-nm laser, as well as the PE filter (584/42 nm) and FITC filter (530/30 nm), respectively. At least 50,000-100,000 events were collected per sample for all flow cytometry studies. Total cell counts and the percentages of fluorescent OVCAR-8-DsRed2 and NCI/ADR-RES-EGFP cells were determined using FlowJo V10 flow cytometry analysis software.

Combination of olaparib and photodynamic therapy

A total of 5×10^4 OVCAR-8-DsRed2 and NCI/ADR-RES-EGFP cells were mixed in equal numbers and cultured in 35-mm Petri dishes to allow overnight attachment at 37 °C in a humidified atmosphere containing 5% CO_2. To initiate one cycle of combination treatment, cells were incubated with olaparib (10 or 25 μM) and photosensitizer (0.25 μM of BPD or (16:0)LysoPC-BPD) for 24 h prior to red light activation at 0.5 J/cm^2 (690 nm, 10 mW/cm^2, Modulight). Following light activation, cells were cultured for another 24 h to complete one cycle of treatment. The same combination treatments were repeated for up to 3 cycles in selected dishes. By the end of each treatment cycle (i.e., on the 3rd, 5th, and 7th experimental day), treated cells or controls were detached by trypsin and collected for determination of the total cell counts or the percentages of fluorescent cells as described above. Controls include no treatment, olaparib alone, and PDT alone for 1-3 cycles. We have selected 25 μM of olaparib because it reduces the total number of co-cultured cells by 50% after one cycle of treatment. A sub-lethal olaparib dose of 10 μM was used to further explore the combination effects between PDT and olaparib.

Clonogenic assay

Cell survival after treatment was evaluated *via* the clonogenic assay. Plating of OVCAR-8-DsRed2 and NCI/ADR-RES-EGFP cells (1:1 mixture at 1000 or 500 cells/35-mm dish) before treatment was used to determine the sensitivity and efficiency of different combination treatment cycles and controls as described above. By the end of each treatment cycle, cells were washed twice with PBS and cultured in a fresh medium for colony formation. On the eighth experimental day, cells were fixed with 4% formaldehyde in PBS for 30 min, followed by 0.5% crystal violet staining for 1 h at room temperature. The dishes were air-dried after washing out the dye, and the images of each dish were taken for cell counting using ImageJ software. After counting the clones, plating efficiency (PE) and survival fraction (SF) were calculated using the following equations: (1) PE = 100% × number of colonies formed/number of cells seeded, and (2) SF = number of colonies formed after treatments/(number of cells seeded × PE).

Immunoblotting

A 1:1 mixture of OVCAR-8-DsRed2 and NCI/ADR-RES-EGFP cells were plated in 35 mm dishes at a density of 5×10^4 cells per dish. After adhering overnight, cells were treated with either 25 μM of olaparib, 0.25 μM of photosensitizer (BPD or (16:0)LysoPC-BPD), or their combination regimens. After a 24 h incubation, cells were light-activated with a 690 nm laser (0.5 J/cm^2, 10 mW/cm^2, Modulight). At 24 h following PDT, cell lysates were collected in radioimmunoprecipitation assay buffer (RIPA buffer) supplemented with 1% phosphatase and protease inhibitor cocktail. Protein lysates (20 μg) of each sample were separated on a NuPAGE 4–12% precast Bis-Tris gel (Mini-tank system, ThermoFisher) and transferred onto a polyvinylidene difluoride (PVDF) membrane. After blocking in 5% BSA or milk in tris-buffered saline with 0.1% Tween® 20 Detergent (TBST), the blot was incubated with primary antibody against PARP (#9542, CST), *p*-H_2AX (#05636, Millipore), or β-actin (#4970, CST) overnight at 4 °C followed by incubation with secondary antibody for 1 h at room temperature. Visualization of protein bands was achieved by chemiluminescence (SuperSignal, ThermoFisher) using the FluorChem E imaging system (ProteinSimple). β-actin served as a loading control.

Statistical analysis

All experiments were repeated at least three times. Specific tests and number of repeats are indicated in the Fig. captions. Results are shown with mean ± standard error of the mean. Statistical analyses were performed using GraphPad Prism (GraphPad Software). Reported *p* values are two-tailed. One-way analysis of variance (ANOVA) analysis and appropriate post hoc tests were applied to avoid type I errors.

Results

Growth kinetics of resistant and sensitive cell populations

A previous study showed that the fluorescent OVCAR-8-DsRed2 and NCI/ADR-RES-EGFP cell lines retain the phenotypic and genotypic characteristics of their parental lines, OVCAR-8 and NCI/ADR-RES, respectively [36]. NCI/ADR-RES is a drug-selected, P-gp-overexpressing variant of OVCAR-8 as confirmed *via* bioinformatic analysis [37,38]. Fig. 1A shows the morphological and fluorescent characteristics of OVCAR-8-DsRed2 and NCI/ADR-RES-EGFP cells assessed using an automated microscope. Both cell lines exhibit strong fluorescence intensity in cultures. Automatic cell counter and cell size analysis revealed that the size of NCI/ADR-RES-EGFP cells is around 15–24 μm, which is slightly larger than that of OVCAR-8-DsRed2 cells (~12–18 μm). Western blotting confirmed that P-gp expression is much higher in the resistant NCI/ADR-RES-EGFP cell line compared to the OVCAR-8-DsRed2 line (Fig. 1B). These cells, therefore, represent ovarian cancer subpopulations of drug sensitive (OVCAR-8-DsRed2) and resistant (NCI/ADR-RES-EGFP) variants. The growth of each variant was

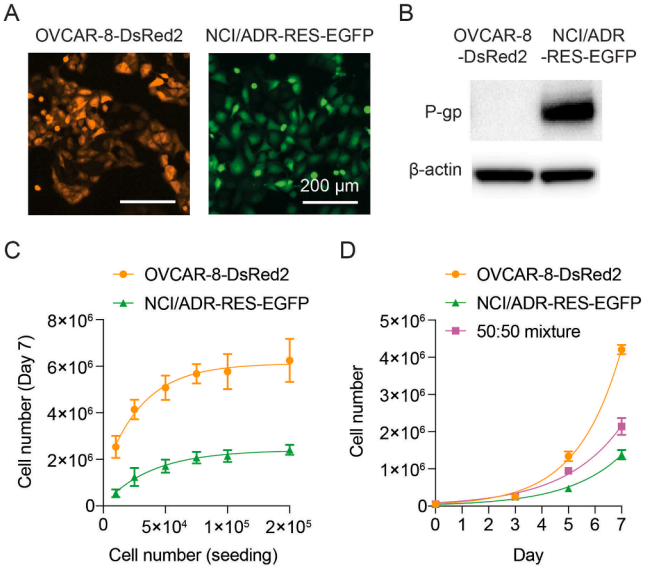

Fig. 1. Characterization of OVCAR-8-DsRed2 and NCI/ADR-RES-EGFP cell lines. (A) Representative fluorescence images of OVCAR-8-DsRed2 (pseudo color orange) and NCI/ADR-RES-EGFP (pseudo color green) cells. Scale bar: 200 μm. (B) Western blotting confirmed the overexpression of P-gp in the NCI/ADR-RES-EGFP cell line. (C) The number of OVCAR-8-DsRed2 and NCI/ADR-RES-EGFP cells was measured after 7 days of culture at different seeding densities ranging from 1×10^4 to 2×10^5. (D) The growth curves of OVCAR-8-DsRed2 cells, NCI/ADR-RES-EGFP cells, and their mixture at 1:1 ratio. The cell seeding density was fixed at 5×10^4 cells per 35-mm dish. Results are expressed as mean ± standard error of the mean.

monitored over one week in 35-mm Petri dishes at different cell seeding densities ranging from 10,000 to 200,000 cells. The growth curves were generated by quantifying the total cell number using the automated cell counter (Fig. 1C). Cell growth was faster in OVCAR-8-DsRed2 than in NCI/ADR-RES-EGFP as described previously [36]. Additionally, cells plated at a density greater than 50,000 plateaued upon reaching confluency. Prior to reaching confluency, the cell number of OVCAR-8-DsRed2 was roughly 3 times higher than that of NCI/ADR-RES-EGFP cells following one week of culture. The seeding density of 50,000 cells per 35-mm dish was chosen for further co-culture experiments of OVCAR-8-DsRed2 and NCI/ADR-RES-EGFP (Fig. 1D). After one week of culture, the 1:1 ratio mixed cell population (Fig. 1D, pink solid square) had a total of 2.1±0.2 million cells, which lies between the monocultures of OVCAR-8-DsRed2 (4.2±0.1 million cells) and NCI/ADR-RES-EGFP (1.4±0.1 million cells).

The sensitive population dominates the co-culture in the absence of treatment

Monitoring population dynamics in a co-culture system is necessary for understanding the consequences of heterogeneous cancer evolution. Here, we quantify the population ratio of OVCAR-8-DsRed2 and NCI/ADR-RES-EGFP in co-culture using fluorescence-activated cell sorting (FACS) throughout a two-week culture period. Fig. 2A shows the dynamic evolution of the resistant and sensitive subpopulations in co-culture. The sensitive variant OVCAR-8-DsRed2 quickly begins dominating the population within days of culture and is at around 95% of the population by two weeks. These changes in ratio become statistically significant in as early as five days (Fig. 2B). After one week of co-culture, there were approximately 4.8 times more OVCAR-8-DsRed2 cells than NCI/ADR-RES-EGFP cells. This number increased to about 20 times more OVCAR-8-DsRed2 cells by the end of the two-week culture. Representative fluorescence images (Fig. 2C) also confirm that without treatment, P-gp-negative OVCAR-8-DsRed2 cells (pseudocolor, orange) dominate the culture and drive P-gp-positive NCI/ADR-RES-EGFP (pseudocolor, green) cells to less than 22% at day 7.

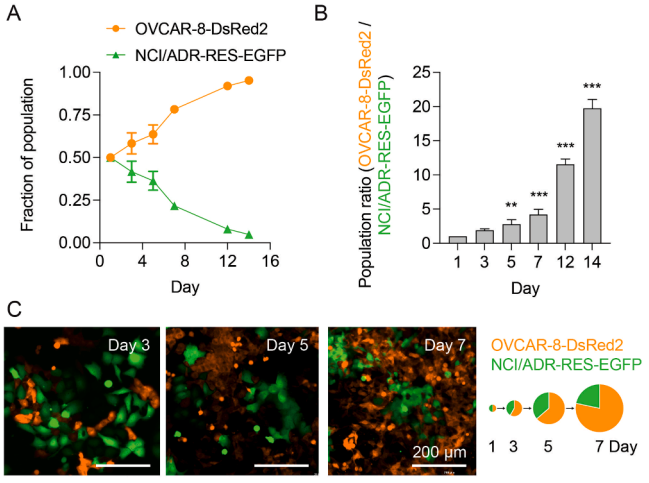

Fig. 2. Growth kinetics of OVCAR-8-DsRed2 and NCI/ADR-RES-EGFP co-cultures. (A) Without treatment, OVCAR-8-DsRed2 cells dominated the culture and drove NCI/ADR-RES-EGFP cells toward extinction. (B) Analysis of the population ratio over time showed that the number of OVCAR-8-DsRed2 cells was around 20 times that of NCI/ADR-RES-EGFP by day 14. Asterisks denote significance compared to the day 1 population ratio (**$p<0.01$, ***$p<0.001$, one-way ANOVA with Tukey's multiple comparisons test). Results are expressed as mean ± standard error of the mean. (C) Representative fluorescence images of the co-culture on days 3, 5, and 7 show the gradual overtaking of the NCI/ADR-RES-EGFP cells by the OVCAR-8-DsRed2. Scale bar: 200 μm. The succession of pie charts corresponding to these microscope images depict the actual population ratios. The size of the pie charts represents the total number of cells normalized to day 1.

Combination of olaparib and PDT is effective in reducing ovarian cancer cell number

Next, we evaluated the effects of olaparib, PDT, and their combination on the number of cells in the co-culture model of OVCAR-8-DsRed2 and NCI/ADR-RES-EGFP. The treatments were performed for up to three cycles, where each cycle lasted for two days (Fig. 3A). PDT was accomplished by exploiting two kinds of photosensitizers, BPD and (16:0)LysoPC-BPD, both of which exhibited similar photochemical behavior as described previously [24]. The number and ratio of the population subclones were determined using the automated cell counter and FACS at the end of each treatment cycle, and at the end of the drug-free culture. These data are shown in Figs. 3 and 4 for 25 μM and 10 μM of olaparib, respectively. These data uniquely provide not only quantification of total cell number, but also the relative populations of the sensitive OVCAR-8-DsRed2 (P-gp negative) and resistant

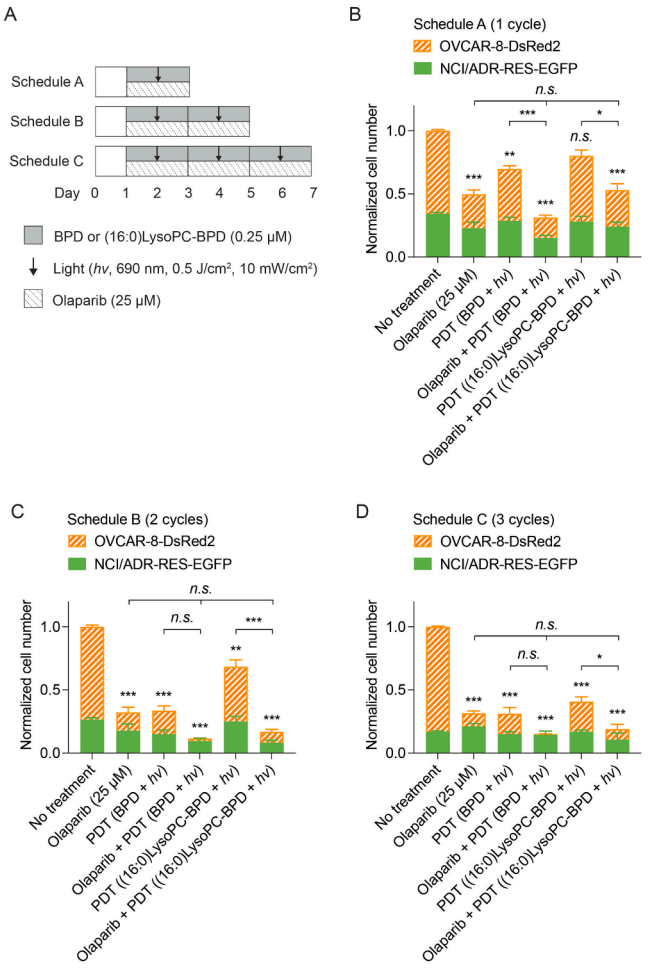

Fig. 3. Combination of olaparib (25 μM) and photodynamic therapy (PDT) in a co-culture model of ovarian cancer. (A) Co-cultures of OVCAR-8-DsRed2 and NCI/ADR-RES-EGFP were treated with olaparib (25 μM), BPD or (16:0)LysoPC-BPD (0.25 μM) with light (690 nm, 0.5 J/cm^2, 10 mW/cm^2), and their combinations. The normalized numbers of OVCAR-8-DsRed2 and NCI/ADR-RES-EGFP cells were reported after (B) 1 cycle, (C) 2 cycles, and (D) 3 cycles of treatment. Results shown are the mean ± standard error of the mean. Asterisks denote significance compared to the no treatment group or amongst the indicated groups at each time point (*$p<0.05$, **$p<0.01$, ***$p<0.001$, one-way ANOVA with Tukey's multiple comparisons test). "*n.s.*" indicates not significant ($p>0.05$).

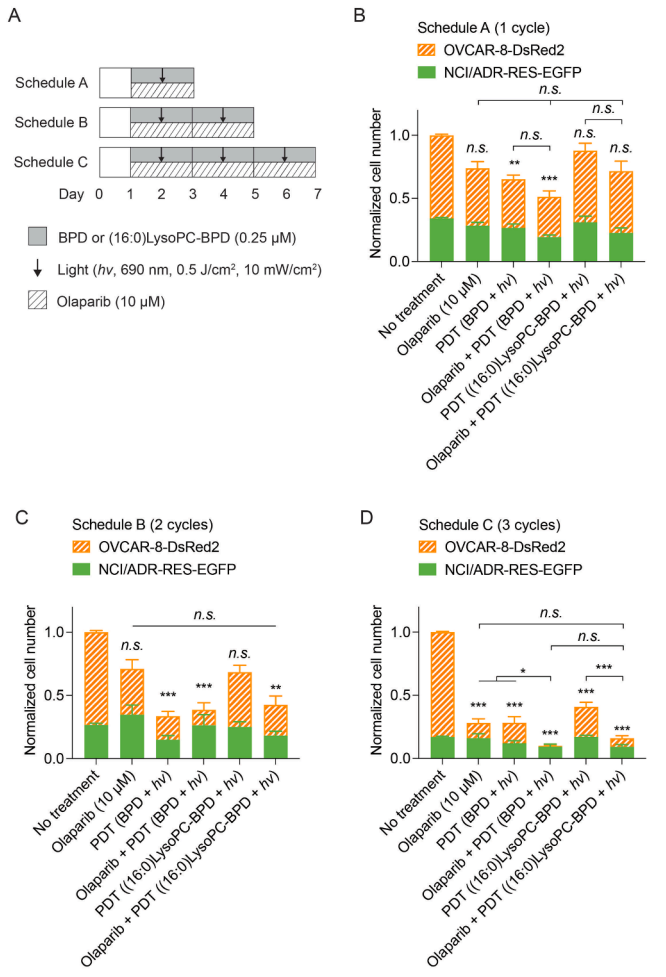

Fig. 4. Combination of olaparib (10 μM) and photodynamic therapy (PDT) in a co-culture model of ovarian cancer. (A) Co-cultures of OVCAR-8-DsRed2 and NCI/ADR-RES-EGFP were treated with olaparib (10 μM), BPD or (16:0)LysoPC-BPD (0.25 μM) with light (690 nm, 0.5 J/cm^2, 10 mW/cm^2), and their combinations. The normalized numbers of OVCAR-8-DsRed2 and NCI/ADR-RES-EGFP cells were reported after (B) 1 cycle, (C) 2 cycles, and (D) 3 cycles of treatment. Results shown are the mean ± standard error of the mean. Asterisks denote significance compared to the no treatment group or amongst the indicated groups at each time point (*p<0.05, **p<0.01, ***p<0.001, one-way ANOVA with Tukey's multiple comparisons test). "*n.s.*" indicates not significant (p>0.05).

NCI/ADR-RES-EGFP (P-gp positive) cell lines. This demonstrates that our co-culture system is an appropriate model to study the evolutionary dynamics of P-gp expression in diverse ovarian cancer cell populations.

Fig. 3B shows that one cycle of 25 μM olaparib alone and BPD-based PDT alone reduced the total cell number by roughly 50% and 30%, respectively. On the other hand, one cycle of (16:0)LysoPC-BPD-based PDT only decreased the total cell number by less than 20%, and it was found not significantly different than the no treatment group (p>0.05). These results are consistent with our earlier work, as we have previously shown that (16:0)LysoPC-BPD-based PDT is up to 4 times less phototoxic in cancer cells than BPD due, in part, to the reduced uptake of (16:0) LysoPC-BPD by cells [24]. One cycle of 25 μM olaparib and BPD-PDT significantly reduced the total cell number by ~70% compared to no treatment (p<0.001). However, one cycle of combined olaparib and (16:0)LysoPC-BPD-based PDT only lowered the total cell number by ~50% compared to no treatment (p<0.001). Further statistical analysis shows that one cycle of combined olaparib and PDT (with either BPD or (16:0)LysoPC-BPD) is not significantly superior to olaparib alone at 25 μM (p>0.05). These results motivated us to investigate multicycle treatments (Fig. 3C and 3D) and use a lower dose of olaparib at 10 μM (Fig. 4).

This combinational effect becomes increasingly pronounced at later treatment cycles. Two (Fig. 3C) and three (Fig. 3D) cycles of combined olaparib (25 μM) and PDT (with either BPD or (16:0)LysoPC-BPD) significantly reduced the total cell number by 80-90% (p<0.001). However, these combinations are not significantly more effective than olaparib at 25 μM (p>0.05). Using a lower olaparib dose of 10 μM, one cycle and two cycles of combined olaparib and PDT using either photosensitizer formulation only decreased the total cell number by ~38% and ~59%, respectively (Fig. 4B and 4C). Interestingly, three cycles of low-dose olaparib treatment (10 μM) and BPD-based PDT reduced the total cell number by ~90%, and this combination was found to be significantly better than monotherapies at reducing overall cell number (p<0.05, Fig. 4D). Similarly, three combination cycles of low dose olaparib (10 μM) with (16:0)LysoPC-BPD-based PDT was found to be effective, reducing the total cell number by ~84%.

Combination of olaparib and (16:0)LysoPC-BPD-based PDT mitigates possible selection pressure

Despite providing large reductions in the total cell number, the combination of olaparib and PDT was more effective in reducing the number of OVCAR-8-DsRed2 cells than NCI/ADR-RES-EGFP cells. Flow cytometry analysis showed that multiple cycles of olaparib, or PDT alone, reduce the number of sensitive OVCAR-8-DsRed2 cells by 74–87%, but only kill fewer than 43% of resistant NCI/ADR-RES-EGFP cells (Figs. 3 and 4). The combination of olaparib and BPD-based PDT for two or three cycles killed nearly all (>95%) OVCAR-8-DsRed2 cells, leaving behind the drug resistant cells to dominate the co-culture. Interestingly, the multicycle combination of olaparib and (16:0) LysoPC-BPD-based PDT did not completely eradicate the sensitive OVCAR-8-DsRed2 cells. These observations motivated us to further analyze the cell population ratios at different time points during the combination treatment (Fig. 5A). The OVCAR-8-DsRed2/NCI/ADR-RES-EGFP population ratio in the no treatment group steadily increases from 1 to ~5 over 7 days (Fig. 5B and 5C). In contrast, treatment with 10 μM and 25 μM olaparib resulted in a significant reduction of the OVCAR-8-DsRed2/NCI/ADR-RES-EGFP population ratio from 1 to 0.48 and 0.74, respectively, over 7 days. The OVCAR-8-DsRed2/NCI/ADR-RES-EGFP population ratio remained relatively steady between 1 and 1.67 after one to three cycles PDT. Combination treatment with olaparib (10 or 25 μM) and BPD-PDT resulted in an average OVCAR-8-DsRed2/NCI/ADR-RES-EGFP population ratio of 0.04 at day 7, demonstrating near-complete dominance of the treatment resistant population. Interestingly, (16:0)LysoPC-BPD-based PDT combined with olaparib resulted in 10-18-fold higher OVCAR-8-DsRed2/NCI/ADR-RES-EGFP population ratios of 0.4–0.74 at day 7 compared to the combination with BPD-based PDT and olaparib.

Clonogenic assays show the inhibition of clonogenic survival of human ovarian cancer cells by the olaparib and PDT combination

To determine the long-term cytotoxic effects of olaparib (10 μM), PDT, and their combination, we conducted clonogenic assays for each cycle treatment (Fig. 6A-D). Figs. 6B-6D show the cytotoxicity of olaparib monotherapy increases in a treatment cycle-dependent manner. One, two, and three cycles of olaparib reduced the number of ovarian cancer colonies by 46%, 70%, and 75%, respectively. BPD-based PDT alone also reduced the number of ovarian cancer colonies by 10–25% after each treatment cycle. Additionally, one cycle of BPD-based PDT in combination with olaparib significantly reduced the surviving fraction by 33–52% compared to either monotherapy. However, after two or three treatment cycles, the combination of BPD-based PDT and olaparib did not significantly (p>0.05) improve outcomes compared to olaparib alone. Similar to the results observed in Figs. 3 and 4, the clonogenic

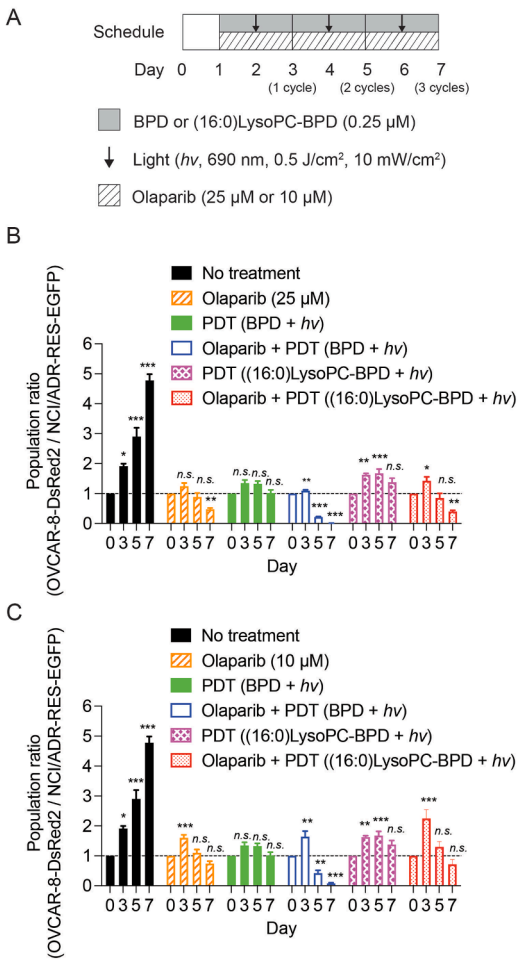

Fig. 5. Analysis of population ratio of OVCAR-8-DsRed2 over NCI/ADR-RES-EGFP at days 0, 3, 5, and 7 (A) over three cycles of combination treatments using PDT and (B) 25 μM of olaparib or (C) 10 μM of olaparib. Results shown are the mean ± standard error of the mean. Asterisks denote significance compared to the population ratio at day 0 (*p<0.05, **p<0.01, ***p<0.001, one-way ANOVA with Tukey's multiple comparisons test). "*n.s.*" indicates not significant (p>0.05).

assay showed that (16:0)LysoPC-BPD is less photo-cytotoxic than BPD under the same light irradiation condition. The combination of (16:0) LysoPC-BPD-based PDT and olaparib modestly inhibited the clonogenic survival of ovarian cancer cells to 53%, 27% and, 19% after one, two, and three treatment cycles, respectively, compared to the no treatment control. While the combination of (16:0)LysoPC-BPD-based PDT and olaparib did not outperform the combination of BPD-based PDT and olaparib, we know based on Fig. 5 that the use of (16:0)LysoPC-BPD could help reduce the selective advantage of resistant cells.

Combination of olaparib and PDT enhances DNA damage in human ovarian cancer cells

To elucidate the cell death mechanisms of olaparib combined with PDT, we examined the expression of p-H_2AX and cleaved PARP in an ovarian cancer co-culture model of OVCAR-8-DsRed2 and NCI/ADR-RES-EGFP using western blots (Fig. 7A). Quantitative analysis showed no significant changes in PARP expression after PDT (with either BPD or (16:0)LysoPC-BPD), olaparib, or their combination treatments (Fig. 7B). PARP cleavage was observed in the presence of olaparib, both alone and in combination with BPD-based PDT or (16:0)LysoPC-BPD-based PDT (Fig. 7C). The elevated levels of PARP cleavage in these three groups were comparable, suggesting that olaparib dominated the PARP cleavage effects in the combination regimen. The expression of p-H_2AX in cancer cells significantly elevated in the combination regimen compared to the no treatment and monotherapy controls (Fig. 7D). This suggests that the combination of olaparib and PDT could induce a more severe DNA injury in ovarian cancer cells than either treatment alone.

Discussion

High-grade serous ovarian cancer is the most lethal gynecologic cancer [39]. Resistance to conventional agents, such as platinum- and taxane-based chemotherapies, remains a key reason for the persistently grim statistics. Increased expression of P-gp has been seen in drug resistant ovarian cancer lines [40,41]. Several clinical studies have also shown that P-gp is expressed in ovarian tumors treated with drugs that are substrates of P-gp, but not in untreated tumors [42-44]. In 2014, the Food and Drug Administration (FDA) first approved olaparib (LYNPARZA®) for the treatment of *BRCA*-mutated, advanced ovarian cancer, and it was later approved for breast, pancreatic, and prostate cancers in 2018, 2019, and 2020, respectively. Other PARP inhibitors have also received FDA-approval for the treatment of ovarian cancer (niraparib, rucaparib) and prostate cancer (rucaparib). Olaparib and several other PARP inhibitors are P-gp substrates [16]. However, the impact of multicycle olaparib therapy on P-gp expression in ovarian cancer remains relatively unknown. Most clinical and pre-clinical studies of P-gp in tumors still rely on static histopathological characterization, such as immunohistochemistry and quantitative RT-PCR [4]. In the landscape of cancer evolution [7,45], the need to frequently adjust treatment conditions based on a tumor's response to therapy mandates a conceptual shift from "static characterization" techniques to "dynamic monitoring" of tumor behavior. *In vitro* multi-fluorescent co-culture systems are ideal models to study the population dynamics of sensitive and resistant cancer cells as they evolve through disease progression and treatment [36]. Using a dual-fluorescent co-culture model of human high-grade serous ovarian cancer cells, we showed that sensitive cells (P-gp-negative) dominate the co-culture and drive resistant cancer cells (P-gp-positive) toward extinction after 2 weeks of culture in the absence of treatment (Fig. 2). Similar results were observed by Grolmusz and colleagues in a 3D co-culture model of sensitive and resistant breast cancer cells [46]. It has also been suggested that multidrug resistant cancer cells require additional energy to maintain and synthesize P-gp [47–49], thus likely trading-off the nonessential functions like proliferation [50]. This significant energetic cost of resistance could potentially explain why sensitive ovarian cancer cells (OVCAR-8-DsRed2) have a higher proliferation rate than resistant cells (NCI/ADR-RES-EGFP). Fig. 1 shows that, at the same initial seeding density, the number of mono-cultured OVCAR-8-DsRed2 cells is ~3 times higher than mono-cultured NCI/ADR-RES-EGFP after 7 days. In contrast, in the co-culture model (Fig. 2), the number of OVCAR-8-DsRed2 cells is ~4.8 folds higher than that of NCI/ADR-RES-EGFP. This suggests that the overtaking of NCI/ADR-RES-EGFP by OVCAR-8-DsRed2 in the co-culture may be beyond their differences in doubling time. Consistent with our findings, ovarian cancer cells overexpressing P-gp are typically uncommon in pre-treatment advanced ovarian tumors [51–53].

Increased expression of P-gp has been observed in olaparib-resistant cancer models. Using syngeneic mammary tumor mouse models, Rottenberg et al. showed that *Abcb1a/1b*, which encodes the mouse P-gp, was increased up to 85-fold in over 70% of olaparib-resistant tumors [54]. In their study, P-gp negative tumors responded initially to olaparib but ultimately developed resistance to olaparib along with a 3.6-fold increase in *Abcb1b* expression. Here, we found that exposure of human ovarian cancer cells to olaparib therapy can trigger competitive escape, where populations of sensitive cancer cells are destroyed, leaving behind resistant cancer cells that overexpress P-gp (Figs. 3–5). It is important to note that P-gp positivity in human ovarian cancer specimens can vary from 7% to 93% [4]. Several clinical studies have found higher levels of P-gp in ovarian tumors treated with drugs that are substrates of P-gp,

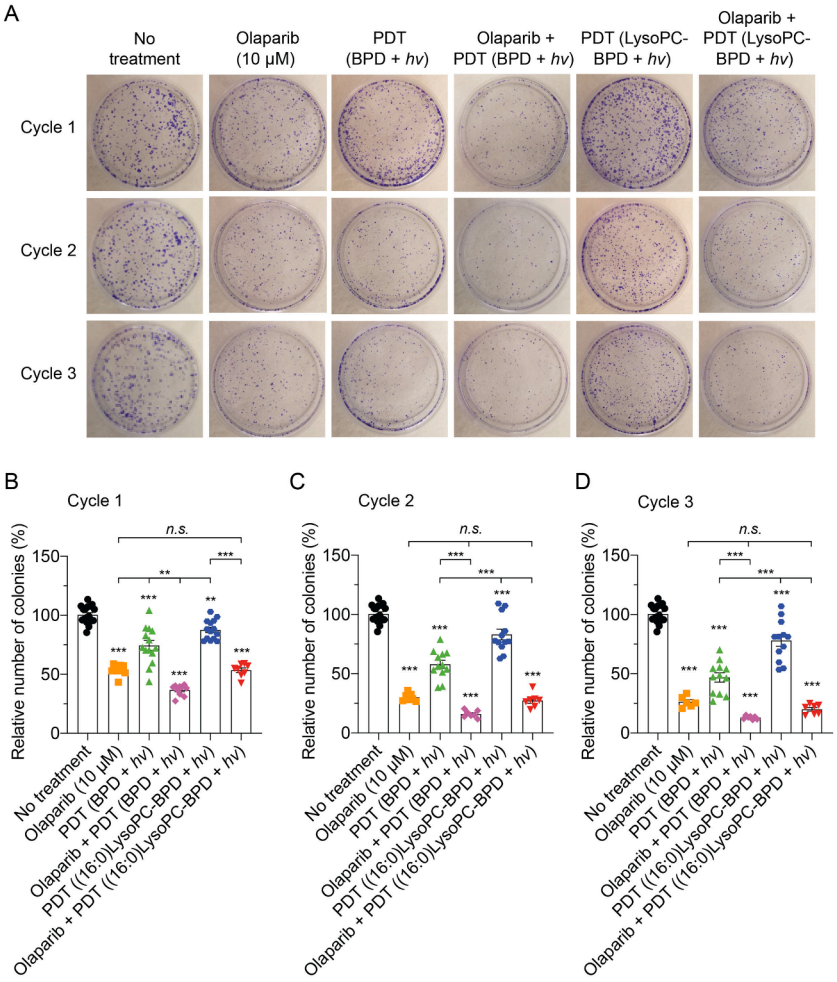

Fig. 6. Combination treatment of olaparib and PDT inhibited the clonogenic survival of human ovarian cancer cells. Co-cultures of OVCAR-8-DsRed2 and NCI/ADR-RES-EGFP at 1:1 ratio were subjected to (i) No treatment, (ii) Olaparib (10 μM), (iii) PDT (0.25 μM BPD with 690 nm light at 0.5 J/cm^2 and 10 mW/cm^2), (iv) PDT (0.25 μM (16:0)LysoPC-BPD with 690 nm light at 0.5 J/cm^2 and 10 mW/cm^2), and (v) combinations of olaparib and PDT for 1-3 cycles. (A) Representative images are shown from clonogenic assays for each cycle of treatment. Cells were cultured for eight days post-treatment prior to crystal violet staining. (B-D) Survival fraction (SF) of the clones, shown as relative number of colonies, was calculated after each cycle of treatment using the equation: Survival fraction = number of colonies formed after treatments/(number of cells seeded × plating efficiency). Results shown are the mean ± standard error of the mean. Asterisks denote significance compared to the no treatment group or amongst the indicated groups at each time point (**p<0.01, ***p<0.001, one-way ANOVA with Tukey's multiple comparisons test). "*n.s.*" indicates not significant (p>0.05).

while others reported no differences in P-gp levels in treated versus untreated ovarian tumors [4]. Similarly, some studies found no relationship between high P-gp levels and poor ovarian cancer patient outcomes, while others reported a strong correlation between the two [4]. These inconsistencies may be due to different cancer subtypes, sample sizes, assays for characterization of P-gp, or chemotherapy settings (e.g., adjuvant, neoadjuvant, first-line, etc.). Further studies of the impact of olaparib therapy on P-gp levels in ovarian tumors as well as their relationship with patient survival outcomes in large and well-defined clinical trials are warranted.

Previous studies have shown that P-gp-expressing drug resistant cancer cells exhibit a lower mitochondrial membrane potential compared to drug sensitive cancer cells [49], and resistant cells could be more susceptible to mitochondrial perturbations [18,20]. These studies motivated us to investigate how clinically relevant BPD-based PDT, a mitochondrial targeting modality [22–25], impacts the population dynamics of resistant and sensitive ovarian cancer cells in a co-culture model. While olaparib decreased the population ratio of sensitive to resistant ovarian cancer cells, 3 cycles of PDT alone effectively maintained the population ratio of sensitive to resistant ovarian cancer cells at ~1. These results are consistent with our previous *in vivo* studies showing that BPD-based photodynamic treatment did not select for subpopulations of pancreatic cancer cells with CD44 and CXCR4 stemness markers [33]. Intraperitoneal PDT is an ideal treatment for residual ovarian cancer peritoneal carcinomatosis at laparotomy/laparoscopy due to its superficial therapeutic effects (few millimeters to centimeters). The clinical feasibility of intraperitoneal PDT for peritoneal carcinomatosis at laparotomy has been demonstrated [55–57]. Additionally, multicycle targeted PDT *via* intraperitoneal catheter has also been shown to reduce ovarian tumor (OVCAR5) burden by 89% in mice [58]. Therefore, it is important to point out that, although not statistically significant (P>0.05), we observed a slight decrease in the population ratio between sensitive and resistant ovarian cancer cells by ~0.3 after 3 cycles of PDT. This suggests that PDT could potentially select for resistant cancer cells after repeated applications. Primary cell cultures can be maintained *in vitro* only for a limited period of time before reaching confluency. In view of the clinical successes with daily olaparib therapy [11,14] and promising preclinical outcomes with multicycle PDT [58,59] for ovarian cancer, a longer-term study of the population dynamics between sensitive and resistant ovarian cancer *in vivo* after multiple cycles combined PDT and olaparib is needed and ongoing in the lab.

Nevertheless, the selection pressure imposed by 3 cycles of PDT on ovarian cancer cells remains much lower than that of olaparib therapy. In this study, the combination of olaparib and 3 cycles of BPD-PDT was found to be the most toxic regimen, but also the biggest contributor to MDR, leading to near complete dominance of resistant cells. Here, we showed that replacing BPD with (16:0)LysoPC-BPD in the combination setting mitigates MDR, similar to our previous finding [34]. In Figs. 3 and 4, as well as in our previous studies [24], we have shown that (16:0) LysoPC-BPD is less phototoxic than BPD. This is in part due to the reduced cellular uptake of (16:0)LysoPC-BPD compared to BPD [24]. Therefore, (16:0)LysoPC-BPD-PDT dosing could be further optimized in future work to maximize phototoxicity and mitigate chemotherapy selection pressures.

Poly(ADP-ribose) polymerase 1 (PARP1) is a 113 kDa nuclear enzyme that is involved in DNA damage repair in cells, and plays an

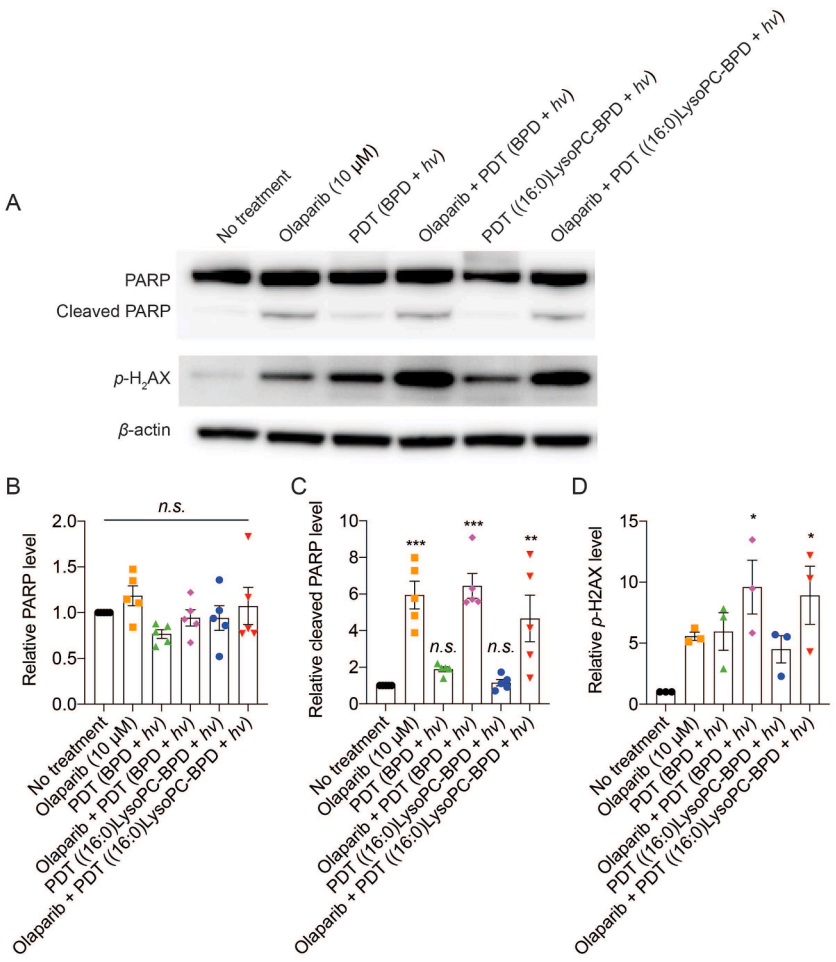

Fig. 7. The combination of olaparib and PDT simultaneously induced the expression of cleaved PARP and *p*-H_2AX in ovarian cancer cells. (A) Monolayer co-cultures of OVCAR-8-DsRed2 and NCI/ADR-RES-EGFP were treated with a single cycle of olaparib, PDT, or their combination. Representative immunoblotting of PARP, cleaved PARP, and *p*-H_2AX in cells subjected to (i) No treatment, (ii) Olaparib (10 μM), (iii) PDT (0.25 μM BPD with 690 nm light at 0.5 J/cm^2 and 10 mW/cm^2), (iv) PDT (0.25 μM (16:0)LysoPC-BPD with 690 nm light at 0.5 J/cm^2 and 10 mW/cm^2), and (v) combinations of olaparib and PDT. The ß-actin serves as a loading control. (B-D) Immunoblot analysis of PARP, cleaved PARP, and *p*-H_2AX in cells at 24 hours post-treatment. Results are mean ± standard error of the mean. Asterisks denote significance compared to the no treatment group (*$p<0.05$, **$p<0.01$, ***$p<0.001$, one-way ANOVA with Tukey's multiple comparisons test). "*n.s.*" indicates not significant ($p>0.05$).

essential role in cell proliferation [12,13]. PARP1 consists of several functional domains, including the DNA-binding domain that contains three Zinc-finger related subdomains (ZnF 1, 2 and 3), the BRCT domain, the WGR domain, and the catalytic domain that contains a helical subdomain (HD) and ADP-ribosyltransferase (ART) catalytic subdomain. When PARP 1 is not bound to the damaged DNA, HD prevents the binding of β-NAD+ to the ART binding site. When ZnF 1, 2 and 3 interact with damaged DNA at single-strand DNA breaks, the remaining PARP1 protein domains assemble onto the PARP1/DNA nucleoprotein structure. This process inactivates the inhibitory function of HD, grants productive β-NAD+ binding by the ART, drives the PARylation of PARP1 substrate proteins to mediate the recruitment of DNA repair effectors for DNA repair, and eventually allows the damaged cell to survive. It is well-established that *BRCA*-mutant cancer cells, which cannot efficiently repair double-strand DNA breaks, are much more sensitive to PARP inhibitors than the *BRCA*-wild type cells [60]. Here, we showed that olaparib induces such synthetic lethality in *BRCA*-defective ovarian cancer cells, increasing the expressions of PARP cleavage and *p*-H_2AX—an indicator of DNA damage (DNA double-strand breaks). We also found that BPD-based PDT, besides targeting the mitochondria, can induce DNA damage as shown by the increased levels of *p*-H_2AX expression. This observation agrees with another report showing that BPD-based PDT can induce DNA fragmentation in the human promyelocytic leukemia HL-60 cell line [61]. While we have shown that PDT can be combined with olaparib to further enhance the DNA damage in *BRCA*-mutant cancer cells, whether the PDT can re-sensitize *BRCA*-wild type cancer cells to PARP inhibitors remains unknow and warrants further investigation. It has been reported that P-gp inhibitors (e.g., verapamil and elacridar) can reverse resistance to PARP inhibitors (e.g., olaparib) in ovarian cancer cells [41]. Hence, another logical next step is to investigate if co-treatment with PDT and P-gp inhibitors further potentiates the anti-tumor activity of olaparib in the P-gp-overexpressing cancer cells.

In summary, we introduce a new combination regimen of olaparib and PDT for *BRCA*-mutated cancer. The use of a dual-fluorescent *in vitro* co-culture model allowed us to better understand the evolutionary dynamics of resistant and sensitive cancer cells during the course of treatment optimization. PDT not only potentiates the DNA-damaging effects of olaparib but, with the lipidated photosensitizer, also may offer a unique solution to mitigate the development of MDR. With an increasing number of studies showing the feasibility and safety of intraperitoneal PDT for treating locally disseminated cancers like advanced stage ovarian cancer [55–57], the combination of intraperitoneal PDT and olaparib treatment merits further investigations in mouse models and in the clinic.

Declaration of Competing Interest

The authors declare that they have no known competing financial interests or personal relationships that could have appeared to influence the work reported in this paper.

Acknowledgments

The authors thank Drs. Michael M. Gottesman and Robert W. Robey (Laboratory of Cell Biology, Center for Cancer Research, National Cancer Institute, National Institutes of Health, Baltimore, MD) for help with cell culture studies and reviewing the manuscript. The fluorescence-

activated cell sorting (FACS) flow cytometry study and western blot imaging were conducted with support from the BioWorkshop hosted by the Fischell Department of Bioengineering at the University of Maryland, College Park.

Funding

This work was supported by the Foundation for Women's Cancer grant (H.-C.H., D.M.R.), the University of Maryland start-up fund (H.-C.H.), the NCI-UMD Partnership for Integrative Cancer Research seed grant (H.-C.H., M.M.G.), and the National Institutes of Health R01CA260340 grant (H.-C.H.).

Ethical statement

No research conducted in patient contained in the manuscript.

Author Contributions

Y.B. and H.-C.H. conceived and designed experiments; Y.B. planned and performed *in vitro* characterizations, cell count study, and flow cytometry analysis; Y.B. and X.P. planned and performed the clonogenic assay and analysis; Y.B., A.S., C.L., and J.R. performed and contributed to the immunoblotting study and analysis. Y.B., A.S., X.P., and H.-C.H. prepared the manuscript. D.M.R. suggested and commented on the design of experiments and translational aspects. All authors contributed to editing the final manuscript.

References

[1] L.M. Merlo, J.W. Pepper, B.J. Reid, C.C. Maley, Cancer as an evolutionary and ecological process, Nat. Rev. Cancer 6 (2006) 924–935.
[2] E. Lengyel, Ovarian cancer development and metastasis, Am. J. Pathol. 177 (2010) 1053–1064.
[3] R.W. Robey, K.M. Pluchino, M.D. Hall, A.T. Fojo, S.E. Bates, M.M. Gottesman, Revisiting the role of ABC transporters in multidrug-resistant cancer, Nat. Rev. Cancer 18 (2018) 452–464.
[4] M.P. Ween, M.A. Armstrong, M.K. Oehler, C. Ricciardelli, The role of ABC transporters in ovarian cancer progression and chemoresistance, Crit. Rev. Oncol. Hematol. 96 (2015) 220–256.
[5] M. Greaves, C.C. Maley, Clonal evolution in cancer, Nature 481 (2012) 306–313.
[6] C. Willyard, Cancer therapy: an evolved approach, Nature 532 (2016) 166–168.
[7] R.A. Gatenby, J.S. Brown, Integrating evolutionary dynamics into cancer therapy, Nat. Rev. Clin. Oncol. 17 (2020) 675–686.
[8] Y. Kim, J. Chen, Molecular structure of human P-glycoprotein in the ATP-bound, outward-facing conformation, Science 359 (2018) 915–919.
[9] Z.L. Johnson, J. Chen, ATP binding enables substrate release from multidrug resistance Protein 1, Cell 172 (2018) 81–89.
[10] I. Manolaridis, S.M. Jackson, N.M.I. Taylor, J. Kowal, H. Stahlberg, K.P. Locher, Cryo-EM structures of a human ABCG2 mutant trapped in ATP-bound and substrate-bound states, Nature 563 (2018) 426–430.
[11] J.A. Ledermann, E. Pujade-Lauraine, Olaparib as maintenance treatment for patients with platinum-sensitive relapsed ovarian cancer, Therap. Adv. Med. Oncol. 11 (2019) 1–18.
[12] A. Ashworth, C.J. Lord, Synthetic lethal therapies for cancer: what's next after PARP inhibitors? Nat. Rev. Clin. Oncol. 15 (2018) 564–576.
[13] C.J. Lord, A. Ashworth, PARP inhibitors, Synthetic lethality in the clinic, Science 355 (2017) 1152–1158.
[14] K. Moore, N. Colombo, G. Scambia, B.G. Kim, A. Oaknin, M. Friedlander, A. Lisyanskaya, A. Floquet, A. Leary, G.S. Sonke, C. Gourley, S. Banerjee, A. Oza, A. González-Martín, C. Aghajanian, W. Bradley, C. Mathews, J. Liu, E.S. Lowe, R. Bloomfield, P. DiSilvestro, Maintenance olaparib in patients with newly diagnosed advanced ovarian cancer, N. Engl. J. Med. 379 (2018) 2495–2505.
[15] L. Henneman, M.H. van Miltenburg, E.M. Michalak, T.M. Braumuller, J.E. Jaspers, A.P. Drenth, R. de Korte-Grimmerink, E. Gogola, K. Szuhai, A. Schlicker, R. Bin Ali, C. Pritchard, I.J. Huijbers, A. Berns, S. Rottenberg, J. Jonkers, Selective resistance to the PARP inhibitor olaparib in a mouse model for BRCA1-deficient metaplastic breast cancer, Proc. Natl. Acad. Sci. U. S. A. 112 (2015) 8409–8414.
[16] D. Lawlor, P. Martin, S. Busschots, J. Thery, J.J. O'Leary, B.T. Hennessy, B. Stordal, PARP Inhibitors as P-glyoprotein Substrates, J. Pharm. Sci. 103 (2014) 1913–1920.
[17] K.M. Pluchino, M.D. Hall, A.S. Goldsborough, R. Callaghan, M.M. Gottesman, Collateral sensitivity as a strategy against cancer multidrug resistance, Drug Resist. Updates: Rev. Comment. Antimicrob. Anticancer Chemother., 15 (2012) 98-105.
[18] A. Ganguly, S. Basu, P. Chakraborty, S. Chatterjee, A. Sarkar, M. Chatterjee, S. K. Choudhuri, Targeting mitochondrial cell death pathway to overcome drug resistance with a newly developed iron chelate, PLoS One 5 (2010) 1–13.
[19] R.H. Xu, H. Pelicano, Y. Zhou, J.S. Carew, L. Feng, K.N. Bhalla, M.J. Keating, P. Huang, Inhibition of glycolysis in cancer cells: a novel strategy to overcome drug resistance associated with mitochondrial respiratory defect and hypoxia, Cancer Res. 65 (2005) 613–621.
[20] H. Wang, Z. Gao, X. Liu, P. Agarwal, S. Zhao, D.W. Conroy, G. Ji, J. Yu, C. P. Jaroniec, Z. Liu, X. Lu, X. Li, X. He, Targeted production of reactive oxygen species in mitochondria to overcome cancer drug resistance, Nat. Commun. 9 (2018) 1–16.
[21] J.P. Celli, B.Q. Spring, I. Rizvi, C.L. Evans, K.S. Samkoe, S. Verma, B.W. Pogue, T. Hasan, Imaging and photodynamic therapy: mechanisms, monitoring, and optimization, Chem. Rev. 110 (2010) 2795–2838.
[22] D. Kessel, Y. Luo, Mitochondrial photodamage and PDT-induced apoptosis, J. Photochem. Photobiol. B 42 (1998) 89–95.
[23] D. Kessel, M. Castelli, Evidence that bcl-2 is the target of three photosensitizers that induce a rapid apoptotic response, Photochem. Photobiol. 74 (2001) 318–322.
[24] C.T. Inglut, Y. Baglo, B.J. Liang, Y. Cheema, J. Stabile, G.F. Woodworth, H.-C. Huang, Systematic evaluation of light-activatable biohybrids for anti-glioma photodynamic therapy, J. Clin. Med. 8 (2019) 1–20.
[25] D. Kessel, J.J. Reiners, Effects of combined lysosomal and mitochondrial photodamage in a non-small-cell lung cancer cell line: the role of paraptosis, Photochem. Photobiol. 93 (2017) 1502–1508.
[26] B.J. Liang, M. Pigula, Y. Baglo, D. Najafali, T. Hasan, H.-C. Huang, Breaking the selectivity-uptake trade-off of photoimmunoconjugates with nanoliposomal irinotecan for synergistic multi-tier cancer targeting, J Nanobiotechnology 18 (2020) 1–14.
[27] I. Rizvi, T.A. Dinh, W. Yu, Y. Chang, M.E. Sherwood, T. Hasan, Photoimmunotherapy and irradiance modulation reduce chemotherapy cycles and toxicity in a murine model for ovarian carcinomatosis: perspective and results, Isr. J. Chem. 52 (2012) 776–787.
[28] M. Broekgaarden, A. Alkhateeb, S. Bano, A.L. Bulin, G. Obaid, I. Rizvi, T. Hasan, Cabozantinib inhibits photodynamic therapy-induced auto- and paracrine met signaling in heterotypic pancreatic microtumors, Cancers (Basel) 12 (2020) 1–16.
[29] H.-C. Huang, S. Mallidi, J. Liu, C.T. Chiang, Z. Mai, R. Goldschmidt, N. Ebrahim-Zadeh, I. Rizvi, T. Hasan, Photodynamic therapy synergizes with irinotecan to overcome compensatory mechanisms and improve treatment outcomes in pancreatic cancer, Cancer Res. 76 (2016) 1066–1077.
[30] M. Pigula, H.-C. Huang, S. Mallidi, S. Anbil, J. Liu, Z. Mai, T. Hasan, Size-dependent tumor response to photodynamic therapy and irinotecan monotherapies revealed by longitudinal ultrasound monitoring in an orthotopic pancreatic cancer model, Photochem. Photobiol. 95 (2019) 378–386.
[31] S. Anbil, M. Pigula, H.-C. Huang, S. Mallidi, M. Broekgaarden, Y. Baglo, P. De Silva, D.M. Simeone, M. Mino-Kenudson, E.V. Maytin, I. Rizvi, T. Hasan, Vitamin D receptor activation and photodynamic priming enable durable low-dose chemotherapy, Mol. Cancer Ther. 19 (2020) 1308–1319.
[32] C. Inglut, K. Gray, S. Vig, J. Jung, J. Stabile, Y. Zhang, K. Stroka, H.-C. Huang, Photodynamic priming modulates endothelial cell–cell junction phenotype for light-activated remote control of drug delivery, IEEE J. Sel. Top. Quantum Electron. 27 (2020) 1–11.
[33] H.-C. Huang, I. Rizvi, J. Liu, S. Anbil, A. Kalra, H. Lee, Y. Baglo, N. Paz, D. Hayden, S. Pereira, B.W. Pogue, J. Fitzgerald, T. Hasan, Photodynamic priming mitigates chemotherapeutic selection pressures and improves drug delivery, Cancer Res. 78 (2018) 558–571.
[34] Y. Baglo, B.J. Liang, R.W. Robey, S.V. Ambudkar, M.M. Gottesman, H.-C. Huang, Porphyrin-lipid assemblies and nanovesicles overcome ABC transporter-mediated photodynamic therapy resistance in cancer cells, Cancer Lett. 457 (2019) 110–118.
[35] B. Stordal, K. Timms, A. Farrelly, D. Gallagher, S. Busschots, M. Renaud, J. Thery, D. Williams, J. Potter, T. Tran, G. Korpanty, M. Cremona, M. Carey, J. Li, Y. Li, O. Aslan, J.J. O'Leary, G.B. Mills, B.T. Hennessy, BRCA1/2 mutation analysis in 41 ovarian cell lines reveals only one functionally deleterious BRCA1 mutation, Mol Oncol 7 (2013) 567–579.
[36] K.R. Brimacombe, M.D. Hall, D.S. Auld, J. Inglese, C.P. Austin, M.M. Gottesman, K. L. Fung, A dual-fluorescence high-throughput cell line system for probing multidrug resistance, Assay Drug Dev. Technol. 7 (2009) 233–249.
[37] D.A. Scudiero, A. Monks, E.A. Sausville, Cell line designation change: multidrug-resistant cell line in the NCI anticancer screen, J. Natl. Cancer Inst. 90 (1998) 862–863.
[38] A.V. Roschke, G. Tonon, K.S. Gehlhaus, N. McTyre, K.J. Bussey, S. Lababidi, D. A. Scudiero, J.N. Weinstein, I.R. Kirsch, Karyotypic complexity of the NCI-60 drug-screening panel, Cancer Res. 63 (2003) 8634–8647.
[39] D.D. Bowtell, S. Bohm, A.A. Ahmed, P.J. Aspuria, R.C. Bast Jr., V. Beral, J.S. Berek, M.J. Birrer, S. Blagden, M.A. Bookman, J.D. Brenton, K.B. Chiappinelli, F. C. Martins, G. Coukos, R. Drapkin, R. Edmondson, C. Fotopoulou, H. Gabra, J. Galon, C. Gourley, V. Heong, D.G. Huntsman, M. Iwanicki, B.Y. Karlan, A. Kaye, E. Lengyel, D.A. Levine, K.H. Lu, I.A. McNeish, U. Menon, S.A. Narod, B.H. Nelson, K.P. Nephew, P. Pharoah, D.J. Powell Jr., P. Ramos, I.L. Romero, C.L. Scott, A. K. Sood, E.A. Stronach, F.R. Balkwill, Rethinking ovarian cancer II: reducing mortality from high-grade serous ovarian cancer, Nat. Rev. Cancer 15 (2015) 668–679.
[40] R. Januchowski, K. Wojtowicz, P. Sujka-Kordowska, M. Andrzejewska, M. Zabel, MDR gene expression analysis of six drug-resistant ovarian cancer cell lines, Biomed. Res. Int. 2013 (2013) (2013) 1–10.
[41] A. Vaidyanathan, L. Sawers, A.L. Gannon, P. Chakravarty, A.L. Scott, S.E. Bray, M. J. Ferguson, G. Smith, ABCB1 (MDR1) induction defines a common resistance mechanism in paclitaxel- and olaparib-resistant ovarian cancer cells, Br. J. Cancer 115 (2016) 431–441.

[42] S.S. Ozalp, O.T. Yalcin, M. Tanir, S. Kabukcuoglu, E. Etiz, Multidrug resistance gene-1 (Pgp) expression in epithelial ovarian malignancies, Eur. J. Gynaecol. Oncol. 23 (2002) 337–340.
[43] R.T. Penson, E. Oliva, S.J. Skates, T. Glyptis, A.F. Fuller, A. Goodman, M.V. Seiden, Expression of multidrug resistance-1 protein inversely correlates with paclitaxel response and survival in ovarian cancer patients: a study in serial samples, Gynecol. Oncol. 93 (2004) 98–106.
[44] T.A. Holzmayer, S. Hilsenbeck, D.D. Von Hoff, I.B. Roninson, Clinical correlates of MDR1 (P-glycoprotein) gene expression in ovarian and small-cell lung carcinomas, J. Natl. Cancer Inst. 84 (1992) 1486–1491.
[45] R.A. Gatenby, O. Grove, R.J. Gillies, Quantitative imaging in cancer evolution and ecology, Radiology 269 (2013) 8–15.
[46] V.K. Grolmusz, J. Chen, R. Emond, P.A. Cosgrove, L. Pflieger, A. Nath, P.J. Moos, A. H. Bild, Exploiting collateral sensitivity controls growth of mixed culture of sensitive and resistant cells and decreases selection for resistant cells in a cell line model, Cancer Cell Int. 20 (2020) 1–13.
[47] H.J. Broxterman, H.M. Pinedo, C.M. Kuiper, L.C. Kaptein, G.J. Schuurhuis, J. Lankelma, Induction by verapamil of a rapid increase in ATP consumption in multidrug-resistant tumor cells, FASEB J. 2 (1988) 2278–2282.
[48] H.J. Broxterman, H.M. Pinedo, C.M. Kuiper, G.J. Schuurhuis, J. Lankelma, Glycolysis in P-glycoprotein-overexpressing human tumor cell lines. Effects of resistance-modifying agents, FEBS Lett. 247 (1989) 405–410.
[49] M.E. Harper, A. Antoniou, E. Villalobos-Menuey, A. Russo, R. Trauger, M. Vendemelio, A. George, R. Bartholomew, D. Carlo, A. Shaikh, J. Kupperman, E. W. Newell, I.A. Bespalov, S.S. Wallace, Y. Liu, J.R. Rogers, G.L. Gibbs, J.L. Leahy, R.E. Camley, R. Melamede, M.K. Newell, Characterization of a novel metabolic strategy used by drug-resistant tumor cells, FASEB J. 16 (2002) 1550–1557.
[50] P.J. Vickers, R.B. Dickson, R. Shoemaker, K.H. Cowan, A multidrug-resistant MCF-7 human breast cancer cell line which exhibits cross-resistance to antiestrogens and hormone-independent tumor growth *in vivo*, Mol. Endocrinol. 2 (1988) 886–892.
[51] K.S. Tewari, A.S. Kyshtoobayeva, R.S. Mehta, I.R. Yu, R.A. Burger, P.J. DiSaia, J. P. Fruehauf, Biomarker conservation in primary and metastatic epithelial ovarian cancer, Gynecol. Oncol. 78 (2000) 130–136.
[52] S.C. Rubin, C.L. Finstad, W.J. Hoskins, P.E. Saigo, D.M. Provencher, M.G. Federici, T.B. Hakes, M. Markman, B.S. Reichman, K.O. Lloyd, Expression of P-glycoprotein in epithelial ovarian cancer: evaluation as a marker of multidrug resistance, Am. J. Obstet. Gynecol. 163 (1990) 69–73.
[53] A.G. van der Zee, H. Hollema, A.J. Suurmeijer, M. Krans, W.J. Sluiter, P. H. Willemse, J.G. Aalders, E.G. de Vries, Value of P-glycoprotein, glutathione S-transferase pi, c-erbB-2, and p53 as prognostic factors in ovarian carcinomas, J. Clin. Oncol. 13 (1995) 70–78.
[54] S. Rottenberg, J.E. Jaspers, A. Kersbergen, E. van der Burg, A.O. Nygren, S. A. Zander, P.W. Derksen, M. de Bruin, J. Zevenhoven, A. Lau, R. Boulter, A. Cranston, M.J. O'Connor, N.M. Martin, P. Borst, J. Jonkers, High sensitivity of BRCA1-deficient mammary tumors to the PARP inhibitor AZD2281 alone and in combination with platinum drugs, Proc. Natl. Acad. Sci. U. S. A. 105 (2008) 17079–17084.
[55] K.A. Cengel, E. Glatstein, S.M. Hahn, Intraperitoneal photodynamic therapy, Cancer Treat. Res. 134 (2007) 493–514.
[56] S. Schmidt, U. Wagner, P. Oehr, D. Krebs, [Clinical use of photodynamic therapy in gynecologic tumor patients–antibody-targeted photodynamic laser therapy as a new oncologic treatment procedure], Zentralbl. Gynakol. 114 (1992) 307–311.
[57] S.M. Hahn, D.L. Fraker, R. Mick, J. Metz, T.M. Busch, D. Smith, T. Zhu, C. Rodriguez, A. Dimofte, F. Spitz, M. Putt, S.C. Rubin, C. Menon, H.W. Wang, D. Shin, A. Yodh, E. Glatstein, A phase II trial of intraperitoneal photodynamic therapy for patients with peritoneal carcinomatosis and sarcomatosis, Clin. Cancer Res. 12 (2006) 2517–2525.
[58] B.Q. Spring, A.O. Abu-Yousif, A. Palanisami, I. Rizvi, X. Zheng, Z. Mai, S. Anbil, R. B. Sears, L.B. Mensah, R. Goldschmidt, S.S. Erdem, E. Oliva, T. Hasan, Selective treatment and monitoring of disseminated cancer micrometastases *in vivo* using dual-function, activatable immunoconjugates, Proc. Natl. Acad. Sci. 111 (2014) E933–E942.
[59] A. Bansal, F. Yang, T. Xi, Y. Zhang, J.S. Ho, *In vivo* wireless photonic photodynamic therapy, Proc. Natl. Acad. Sci. U. S. A. 115 (2018) 1469–1474.
[60] H. Farmer, N. McCabe, C.J. Lord, A.N. Tutt, D.A. Johnson, T.B. Richardson, M. Santarosa, K.J. Dillon, I. Hickson, C. Knights, N.M. Martin, S.P. Jackson, G. C. Smith, A. Ashworth, Targeting the DNA repair defect in BRCA mutant cells as a therapeutic strategy, Nature 434 (2005) 917–921.
[61] D.J. Granville, J.G. Levy, D.W. Hunt, Photodynamic therapy induces caspase-3 activation in HL-60 cells, Cell Death Differ. 4 (1997) 623–628.